Proceedings of the ASME 2010 3rd Joint US-European Fluids Engineering Summer Meeting and 8th International Conference on Nanochannels, Microchannels, and Minichannels
FEDSM-ICNMM2010
August 1-5, 2010, Montreal, Canada

FEDSM-ICNMM2010-30967

EXPERIMENTAL INVESTIGATION OF FLOW PATTERNS, PRESSURE DROP, AND FLOW INSTABILITY DURING FLOW BOILING IN A CROSS-LINKED MICROCHANNEL HEAT SINK

Ayman Megahed, Department of Mechanical and Industrial Engineering
Concordia University, Montreal, Quebec, Canada, a_megah@live.concordia.ca

ABSTRACT

This paper investigates experimentally flow boiling characteristics in a cross-linked microchannel heat sink at low mass fluxes and high heat fluxes. The heat sink consists of 45 straight microchannels with a hydraulic diameter of 248 µm and heated length of 16 mm. Three cross-links, of width 500 µm, are introduced in the present microchannel heat sink to achieve better temperature uniformity and to avoid flow mal-distribution. Flow visualization, flow instability, and two-phase pressure drop measurements are conducted using the dielectric coolant FC-72 for the range of heat flux from 20.1 to 104.2 kW/m^2, mass flux from 109 to 290 kg/m^2.s, and exit quality from 0.02 to 0.65. Flow visualization studies indicate that the observed flow regime is primarily slug. Instability results show that the periods and amplitudes of inlet pressure and outlet saturation temperature oscillations decrease with increasing mass flux. The two-phase pressure drop strongly increases with the exit quality and the two-phase frictional pressure drop increases by a factor of 1.6-2, at $x_{e,o} < 0.3$, as compared with that in the straight microchannel heat sink.

INTRODUCTION

Conventional thermal management methods do not meet microelectronics technology needs in further development, and remain a major bottleneck of this technology. The decreasing size of microelectronics components and the increasing of thermal output density require a dramatic increase of heat dissipation. The next generation of microelectronic devices will require better thermal management techniques through new technologies, such as microchannel heat sinks.

The concept of the microchannel heat sink with a parallel flow was first introduced by Tuckerman and Pease [1]. Since the heat transfer coefficient was inversely proportional to the hydraulic diameter of the channel, the microchannel heat sink was shown to have a much higher heat transfer coefficient than that of a conventional heat sink. Many investigators have studied single-phase heat transfer phenomena within microchannel heat sinks since the pioneering introduction of the microchannel heat sink by Tuckerman and Pease. Recently, flow boiling in microchannel heat sinks has offered numerous benefits over single-phase flow. Advantages include utilizing the latent heat of vaporization, and a nearly constant coolant temperature in the stream-wise direction. However, it also has some drawbacks such as large pressure drop.

Dang et al. [2] explored adiabatic two-phase flow patterns in cross-linked scaled up microchannel heat sinks and compared results with straight microchannel heat sinks. Test sections had 45 rectangular channels and a hydraulic diameter of 1.59 mm. Water and air were used as working fluids, with flow quality ranging from 0 to 0.25, while the mass flux ranged from 41 to 834 kg/m^2.s. Resulting flow patterns were presented in terms of a fractional time function and were classified into the following flow regimes: dispersed, intermittent, and annular. Intermittent flow patterns were slightly more frequent in the cross-linked heat sinks compared to the straight channel heat sinks, while annular flow patterns were less frequent. The latter observation may be due to that the cross links reducing the number of annular flow patterns observed.

Dang and Hassan [3] presented an experimental study on horizontal adiabatic two-phase pressure drop in cross-linked minichannel heat sinks. Water and air were forced through 45 minichannels of D_h = 1.59 mm and 131.3 mm in length with a mass flux and exit quality ranging from 42 - 834 kg/m2.s and 0 - 0.25, respectively. Experiments were carried out for five test sections that differ in number, width, and location of cross-links in addition to a standard straight test section with the same hydraulic diameter. Numbers of cross-links varied from 2 to 6 with a width ranging from 1.58 - 4.76 mm. They found that the cross-links diminish the flow mal-distribution compared to the straight microchannel heat sink design. However, their results showed the number of cross-links has a non distinguished trend on the flow distribution and pressure drop. It was concluded that increasing the cross-link width would enhance flow distribution more significantly than increasing the number of cross-links with the same width. On the other hand, increasing the cross-link width beyond a certain limit does not lead to a more efficient flow distribution.

Xu et al. [4] investigated transient flow boiling patterns and heat transfer behavior in a cross-linked microchannel array at low mass fluxes and high heat fluxes, using liquid acetone as the working fluid. The silicon chip used consisted of an cross-linked microchannel array with 10 triangular microchannels along the longitudinal direction, measuring 300 μm wide and 212 μm deep, with hydraulic diameters of 155.4 μm. Six independent zones were formed by placing 5 trapezoid microchannels across the flow direction, at centerline distances of 3.694 mm. Mass fluxes ranged from 40 - 80 kg/m^2.s, heat fluxes ranged from 107 - 216 kW/m^2, and exit vapor qualities ranged from 0.82 to 1.32. The intercrossed array caused thermally developing flow in each independent zone, and improved heat transfer for single-phase liquid flow. Flow patterns were repeated periodically, with a cycle period of 53 ms. The cycle period was inversely related to the heat flux: higher heat fluxes resulted in shorter cycle periods. The addition of transverse trapezoidal microchannels had little effect on cycle times, while flow patterns were significantly different. Convective heat transfer caused by film evaporation at the liquid-vapor interface was responsible for changes in the heat transfer coefficient: the heat transfer coefficient showed an initial sharp increase (over the first few millimeters) in the single phase liquid flow region, and then decreased rapidly along the direction of flow. Two-phase pressure drop and the effect of cross-links were not investigated in their study.

Muwanga et al. [5] studied flow boiling instability characteristics of straight and cross-linked microchannel heat sinks. Each design consisted of 45 microchannels. Channels were etched in a silicon substrate with a width of 269 μm, height of 283 μm, and a cross-linked width of 269 μm. A glass cover of 500 μm thickness was placed on top of the channels, to allow for visualization, and included eight 1 mm diameter holes for the inlet and eight 1 mm diameter holes for the outlet. Distilled water was used as the working fluid. Tests were carried out at mass fluxes ranging from 91 - 228 kg/m^2.s and inlet temperatures of 70 °C and 80 °C for the straight microchannel heat sink, while an inlet temperature of 70 °C and a mass flux of 137 kg/m^2.s were used for the cross-linked microchannel heat sink. They concluded that the frequency of oscillations depends on the heat flux, flow rate, and inlet subcooling. The inlet temperature oscillation frequency was higher for the straight microchannels than the cross-linked microchannels. Also, the frequency of both designs decreased with increasing heat flux and mass flux. The inlet pressure amplitude, and inlet and outlet temperature amplitudes were observed to increase with increasing heat flux. Results showed that the straight microchannels have higher inlet pressure amplitudes than the cross-linked microchannels, while the straight microchannels have lower inlet and outlet temperature amplitudes than the cross-linked microchannels. Three correlations were developed to predict the experimental results by correlating the dimensional pressure to the boiling number, subcooling number, Weber number, and number of channels.

The present work focuses on the experimental investigation of flow boiling characteristics in cross-linked microchannel heat sinks. This study is aimed at understanding the cross-links effects that contribute to pressure drop, flow instability, and flow regimes for two-phase flow in microchannels under diabatic flow conditions. The microchannel heat sink contains 45 parallel microchannels with a hydraulic diameter of 248 μm (225 μm in width and 276 μm in depth). Three cross-links of width 500 μm have been introduced to offer a greater flow share and to provide a better heat transfer characteristics over straight microchannel heat sinks. Experimental parameters include subcooling temperature of 4 °C, mass flux ranging from 109 to 290 kg/m^2.s, heat flux from 20.1 to 104.2 kW/m^2, and outlet vapor quality from 0.02 to 0.65. Qualitative visualization of two-phase flow regimes is pursued to demonstrate the flow configuration through the cross-links and within the individual sections of the heat sink. Experimental data are presented on flow boiling instability of the inlet pressure and outlet saturation temperature in the inlet and outlet manifolds, respectively. Flow boiling pressure drop characteristics of the cross-linked microchannels heat sink are studied as function of mass flux and vapor quality. Two-phase pressure drop data are combined with previous correlations in the literature for straight microchannel heat sinks for comparison.

EXPERIMENTAL INVESTIGATION

Figure 1 shows a schematic diagram of the experimental rig. The experimental rig is mainly composed of a flow loop, a data acquisition system, and an image acquisition system. Subcooled liquid is supplied from a FC-72 tank through a filter, flowmeter, and preheater before entering the test section. The refrigerant is circulated by a magnetically coupled gear pump (Cole-Parmer), and delivers a maximum flow rate of 290 mL/min. The pump speed can be adjusted manually through an external controller.

The working fluid is first led through a 15 μm micro-filter. Then, the circulated FC-72 flow rate is measured by a nutating digital output flowmeter (DEA Engineering) which operates at a flowrate ranging from 1 to 250 mL/min with an accuracy of ± 0.5 %. Before entering the test section, a preheater is connected to the main loop to preheat the working fluid and to control the subcooling temperature. The preheater is a counter-flow tube-in-tube heat exchanger with FC-72 flowing in the inner tube and distilled heating water flowing in the annulus. A variac is used to control the inlet temperature of the water. After exiting the test section, the two-phase flow of FC-72 continues to the tank after it is condensed. The electric current for joule heating is provided by one BK Precision DC power supplies (Model 1623A), with a voltage range of 0 - 60 V. Fluorinert FC-72 has been employed as the working fluid in the present experiments. It enters the inlet manifold normally subcooled 4 °C below its saturation temperature. The pressure at the outlet of the test section is kept at near atmospheric pressure, where the saturation temperature is 56.1 °C. The saturation properties of FC-72 at the outlet manifold are determined from the measured refrigerant pressure and temperature. Flow boiling heat transfer of FC-72 is influenced by dissolved air. Hence, the test fluid was deaerated completely to remove any dissolved air from the test loop (i.e., tubes, valves, tube joints, and pressure transducers).

Figures 2.a and 2.b show the images of the cross-linked microchannel heat sink. It consists of a silicon substrate, Pyrex

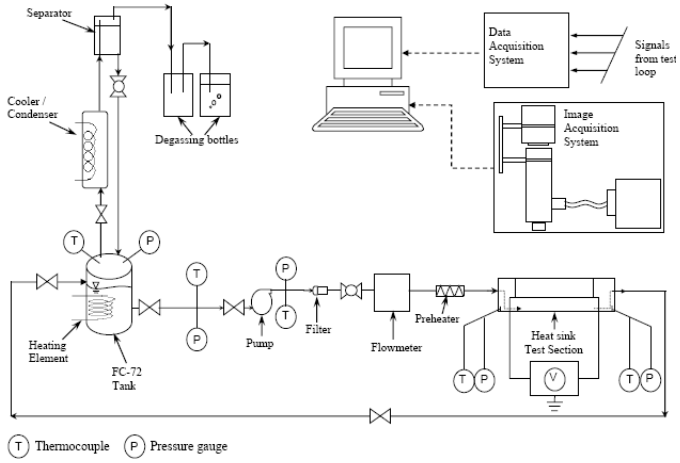

Figure 1. Experimental test facility flow loop [5].

cover, and heating element. Two plenums and 45 rectangular microchannels (225 µm wide, 276 µm deep, 16 mm long) were etched in the 550 µm thick silicon substrate by Deep Reactive Ion Etching (DRIE). Three cross-links of width 500 µm are introduced, in the transverse direction, to divide the microchannels into four equal sections, each measuring 3.625 mm in length. The centerline distance between each section is 4.125 mm. The silicon substrate was then bonded to a 500 µm thick Pyrex cover by anodic bonding to seal the microchannels and plenums. At the same time, the Pyrex cover serves as a transparent cover through which the flow could be visualized. Two holes, each measuring 1 mm in diameter, were manufactured in the Pyrex cover for flow inlet and outlet.

An electrical heater, made of a thin film resistor, has been deposited on the back surface of the silicon substrate to simulate the heat source as shown in Fig 2.b. The heater has a serpentine pattern with a dimension of 0.001 mm in thickness, 1 mm in width and 186 mm in length. This design allows a uniform heating of the surface and reduces the contact resistance between the heater and the wafer. Figure 2.c illustrates the schematic construction of the test section.

The microchannels are visualized by using a high speed 3-CCD analog camera (Sony DXC-9000) equipped with an objective lens 10× (Optem) and a frame grabber installed in a workstation. A data acquisition system was used to collect data from the flow meter, pressure transducers, and thermocouples. These data are monitored and recorded simultaneously while acquiring flow visualization images using Labview software with an area of 640 × 480 pixels for each image. One Optem illuminator is used to provide a high intensity spot of light by an optical fiber light guide. The details of the flow visualization system are also discussed by Muwanga et al. [5]. The Labview software acquires data and records the outputs from the thermocouples, pressure transducers, and flow meter as well as experimental measurements, i.e., current and voltage.

The heat sink is mounted on an acrylic support to facilitate operations and for manipulations. The acrylic support is designed to have a gap to allow for flow visualization and two reservoirs to measure inlet and outlet pressures and temperatures. Two pressure transducers, Omega models PX01C1 and PX02C1, are connected to the inlet and outlet reservoirs to measure the pressure drop across the test section

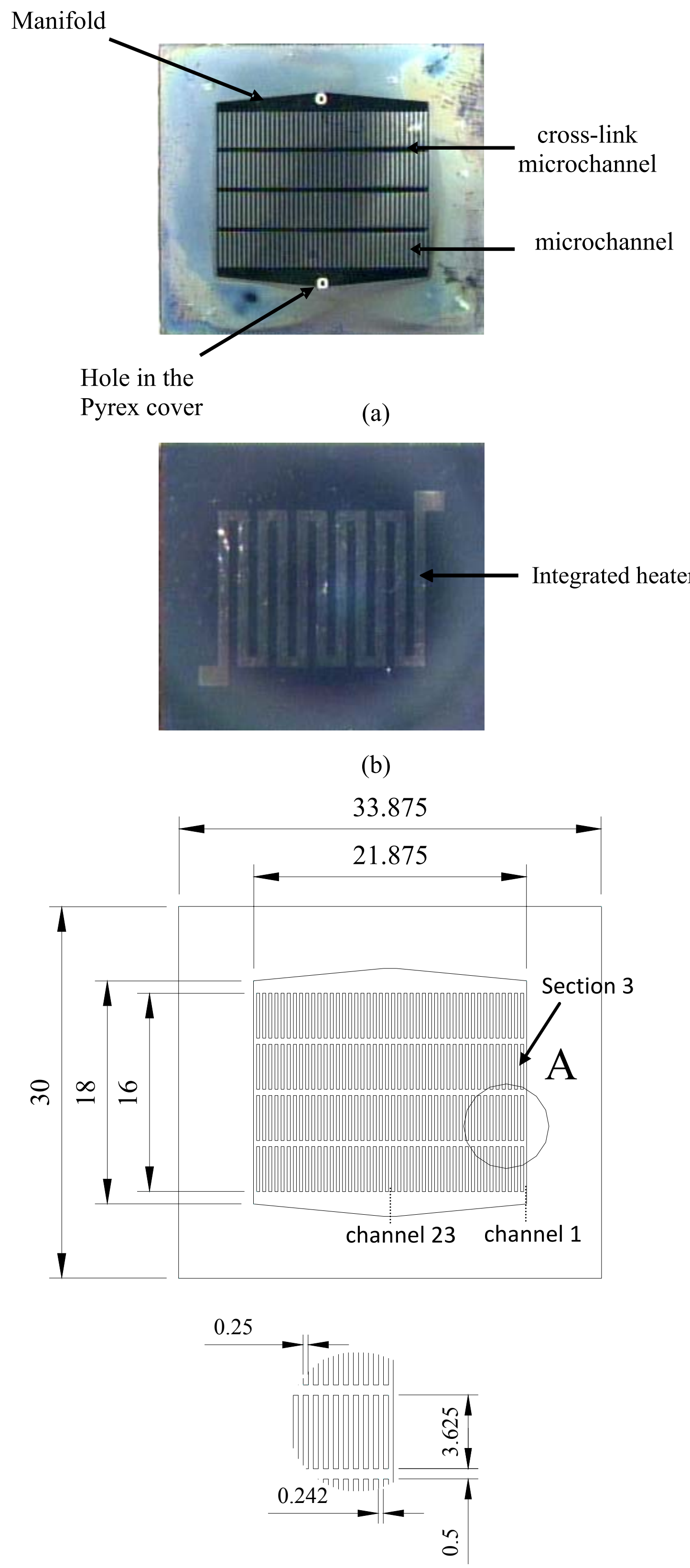

Figure 2. Fabricated cross-linked microchannel heat sink (a) microchannels and Pyrex cover (b) integrated heater on the back (c) Detailed schematic of microchannel heat sink (dimensions are in mm).

with ratings of 517 kPa (75 psi) and 345 kPa (50 psi), respectively. The refrigerant temperatures before and after the test section are measured by a K-type sheathed thermocouples inserted in the inlet and outlet manifolds. Thermochromic Liquid Crystals are utilized to provide detailed non-intrusive measurements of the heat sink surface temperature. Measurements were made at a series of mass fluxes with a constant inlet subcooling temperature of 4 °C.

DATA REDUCTION

The two-phase flow pressure drop in the saturated length of the microchannel is expressed as the sum of the frictional, acceleration and dynamic losses terms as

$$\Delta \boldsymbol{P}_{\mathrm{tp}} = \Delta \boldsymbol{P}_{\mathrm{tp,fr}} + \Delta \boldsymbol{P}_{\mathrm{tp,a}} + \Delta \boldsymbol{P}_{\mathrm{tp,dyn}} \, . \tag{1}$$

The dynamic pressure losses of two-phase flow are the combined effects of two-phase dynamic losses in the microchannel's outlet due to area enlargement and bends. The exit quality can be calculated using the heat balance equation taking into account the sub-cooled region as,

$$\boldsymbol{x}_{\mathrm{e,o}} = \frac{1}{\boldsymbol{h}_{\mathrm{fg}}}\left[\frac{\boldsymbol{Q}_{net}}{\dot{\boldsymbol{m}}} - \boldsymbol{C}_{\mathrm{p}}(\boldsymbol{T}_{\mathrm{sat}} - \boldsymbol{T}_{\mathrm{in}})\right]. \tag{2}$$

The net heat transferred to the fluid (Qnet) is determined as

$$\boldsymbol{Q}_{\mathrm{net}} = \boldsymbol{Q}_{\mathrm{input}} - \boldsymbol{Q}_{\mathrm{loss}} \, , \tag{3}$$

where Qloss is the heat lost during the experiment and Qinput is the input power corresponding to Joule heating. The heat lost from the test section to the ambient is evaluated by the difference between the supplied power and the heat transferred to the refrigerant using a single-phase convective heat transfer run. It was found to be within 2.6 % of the electric heat input at an average refrigerant temperature of 50 °C. The axial conduction heat loss across the heat sink support is estimated as 2.8 %. The net heat flux is found from the following equation

$$\boldsymbol{q} = \frac{\boldsymbol{Q}_{\mathrm{net}}}{\boldsymbol{A}} \, , \tag{4}$$

where A is the total heat transfer area, which can be expressed as:

$$\boldsymbol{A} = (2\boldsymbol{H}_{\mathrm{ch}} + \boldsymbol{W}_{\mathrm{ch}})\boldsymbol{L}_{\mathrm{sec}}\boldsymbol{N}_{\mathrm{ch}}\boldsymbol{N}_{\mathrm{sec}} + 8\boldsymbol{H}_{\mathrm{ch}}\boldsymbol{t}(\boldsymbol{N}_{\mathrm{ch}} - 1) + \boldsymbol{W}_{\mathrm{cr}}\boldsymbol{L}_{\mathrm{cr}}\boldsymbol{N}_{\mathrm{cr}} \tag{5}$$

RESULTS AND DISCUSSION

The flow visualization results are used to obtain a better insight regarding the flow characteristics in the cross-link at G = 109 kg/m^2.s and at $x_{e,o}$ = 0.2. As shown in Fig. 3.a, at the intersection of channel 23 with the mid cross-link (see Fig. 2.c), as the bubble is swept to the cross-link, the bubble is seen to rapidly expand in both directions of the cross-link before it experiences channel confinement again. Thereafter, the bubble goes through several cycles of expansion and contraction caused by the inlet and outlet of the channels as it is conveyed down the channel by the forced flow. In Fig. 3.b at channel 12, the confined bubble spreads out swiftly in the lateral direction. At the same time, a part of the bubble moves away from the channel centerline in the direction of the channels of the lowest mass flux. In Fig. 2.c at channel 1, the vapor bubble gradually expands where a thin layer of liquid is seen trapped between the bubbles. As soon as the confined bubbles expand, the liquid in the slugs between them begins to shrink because of the expanded bubble occupies the cross-link channel.

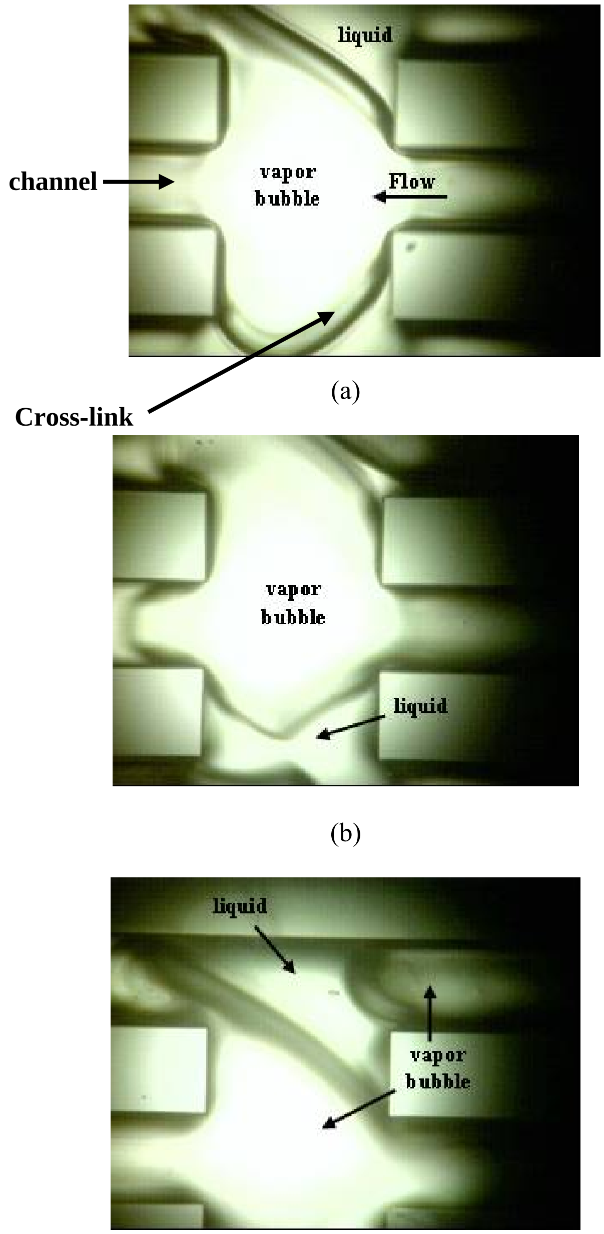

(c)

Figure 3. Observed flow characteristics within the mid cross-link, G = 109 kg/m2.s, $x_{e,o}$ = 0.2, in channels: (a) 23, (b) 12, (c) 1

Qualitative photographs of typical flow patterns observed in the channel segments through the clear Pyrex cover are shown in Figs. 4 and 5 to investigate the effect of cross-links on flow distribution within the test section. Flow visualization is obtained for heat flux ranges from 37 to 69.6 kW/m^2, mass flux ranges from 109 to 195 kg/m2.s, and vapor quality ranges from 0.2 to 0.4. Figure 4 shows the flow distribution as at the intersection of channels 1, 12, and 13 with section 3 (see Fig. 2.c) for a constant mass flux and three different heat fluxes and exit qualities. As the heat flux is increased, the thickness of the trapped liquid layer is observed to decrease and the bubbles start to elongate further (channels 12 and 23). The pattern is seen to exhibit almost the same behavior in the examined channels with increasing exit quality while the mass flux is held constant. In the same figure, presented images also indicate the absence of annular flow regime within the section.

Figure 5 shows the flow visualization in the same channels but at a higher mass flux (G = 195 kg/m^2.s). The constant continuous increase of heat flux results in elongated bubbles, cylindrical in shape, in a continuous slug flow trapping a layer of liquid between them. A notable feature of the slug flow is the bullet-shaped bubbles which can be seen in channel 23 at different values of exit quality as well as in channel 12 at $x_{e,o}$ = 0.4.

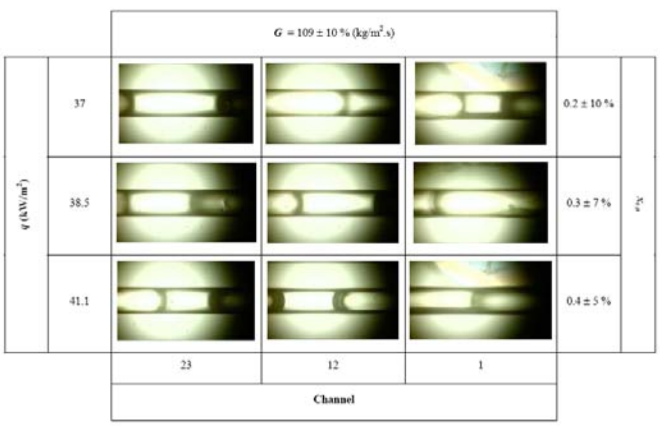

Figure 4. Elongated slug flow at a low mass flux, G = 109 kg/m^{2}s.

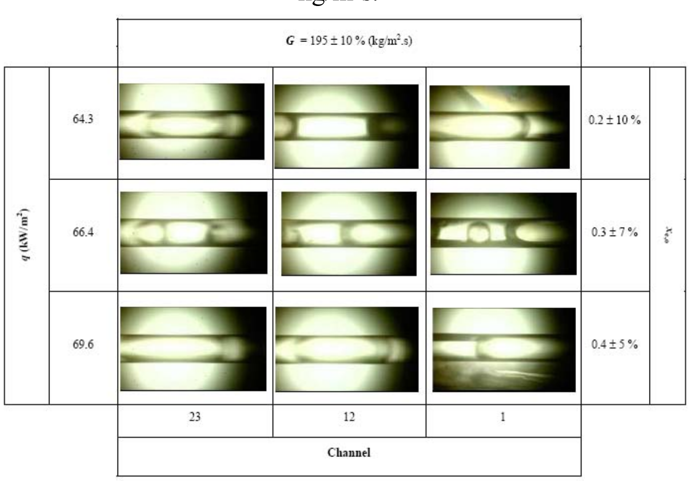

Figure 5. Two-phase flow patterns observed at a high mass flux, G = 195 kg/m^{2}s.

Flow visualization shows that only one major flow pattern exists in channels namely slug flow for all experiments conducted. Bubbly and annular flow regimes are not detected in the examined range of exit quality, heat and mass fluxes. Flow regime transition from slug to annular flow did not take place in the heat sink sections. This behavior could be attributed to the relatively short sections in the cross-linked design compared with the channel length in the straight channel design and due to the effect of transverse flow within the cross-links.

Figure 6 presents the two-phase pressure drop (frictional and acceleration) as a function of the exit vapor quality. These experimental data cover the ranges of $x_{e,o}$ = 0.02 - 0.65, q = 20.1 – 104.2 kW/m^2, and G = 111 - 290 kg/m^{2}s. As shown in the figure, the two-phase pressure drop increases almost linearly with the increase of exit quality at a constant mass flux. It is also clear that the two-phase pressure drop strongly increases with the increase of mass flux at the same exit quality. At low mass fluxes, there is a slight increase in the slope of pressure drop lines with the increase of exit quality. At higher mass fluxes, a sharp increase in pressure drop is clearly seen where the pressure drop lines start diverging. This is attributed to the effect of the cross-links, which add additional pressure losses represented in the abrupt expansion and contraction in the channels' cross-sectional area in addition to the cross flow. Experimental results also indicate significant flow instability and pressure drop fluctuations associated with measurements even after installing a throttling valve prior to the test section. In this regard, Cubaud and Ho [6] and Dukler et al. [7] commented that for slug flow, the data displays much more scatter than in bubbly and annular regimes. Furthermore, Yadigaroglu [8] and Bergles et al. [9] observed that slug flow particularly, as a transition regime from bubbly to annular flow, amplifies flow disturbance. Lee and Pan [10] also reported that an increase in the channel number and channel-to-channel interaction causes an increase in flow instability, which may explain flow instability in the present heat sink design due to the presence of cross-links.

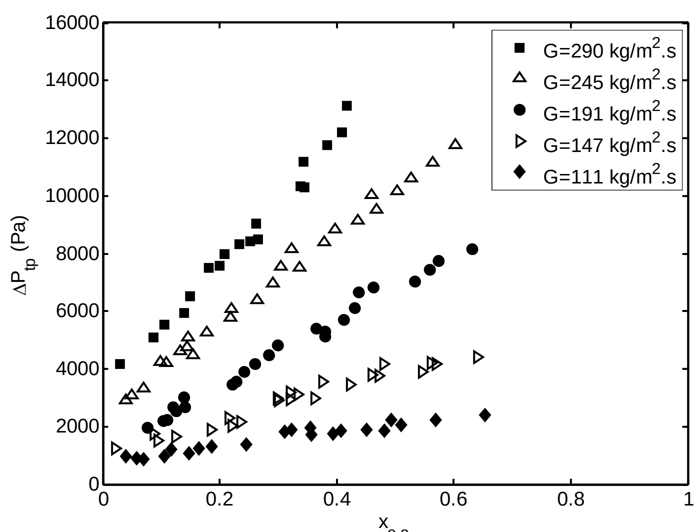

Figure 6. Two-phase pressure drop as function of vapor quality for different mass fluxes.

Many researchers [11-14] have conducted experiments to study pressure drop during two-phase flow in straight microchannel heat sinks. They have demonstrated that the channel size and mass flux are critical parameters in predicting two-phase flow pressure drop in microchannels. Lee and Garimella [14] investigated pressure drop of saturated flow boiling in rectangular microchannels having hydraulic diameters of 160 - 538 μm. They proposed a new correlation for the two-phase multiplier as a function of hydraulic diameter and mass flux. The experimental two-phase frictional pressure drop of the cross-linked design is compared with the above mentioned correlation in order to compare the two-phase pressure drop in the present design with the straight design as shown in Fig. 7. As expected, the two-phase pressure drop through the microchannel heat sink with the cross-links is higher than that of the straight microchannel heat sink at the same mass flux due to the cross-links effect. As seen from Fig. 7, the magnitude of the two-phase pressure drop at low mass flux (G = 111 kg/m^2.s) have a comparable difference between the cross-link and straight microchannel heat sinks (≈ - 30 %). However, the experimental two-phase pressure drop is highly under-predicted at low exit quality ($x_{e,o} < 0.3$) for a higher mass flux. The two-phase pressure drop in the cross-linked design is nearly 1.5 times that in the straight design at $x_{e,o} < 0.3$. At higher vapor quality, ($x_{e,o} > 0.3$), it is seen that the correlation predicts the present data of two-phase pressure drop within - 30 %. This could be explained by that in transitional flow, where slug and plug flow present in the channel, a larger frictional pressure gradient is experienced compared to the higher quality conditions in the straight design where annular flow is established. Huh et al. [15] suggested that very long and fast elongated slugs behave like a semi annular flow. Therefore, as the liquid film thins near the wall, an increase in quality will lead to an increase in two-phase frictional pressure drop.

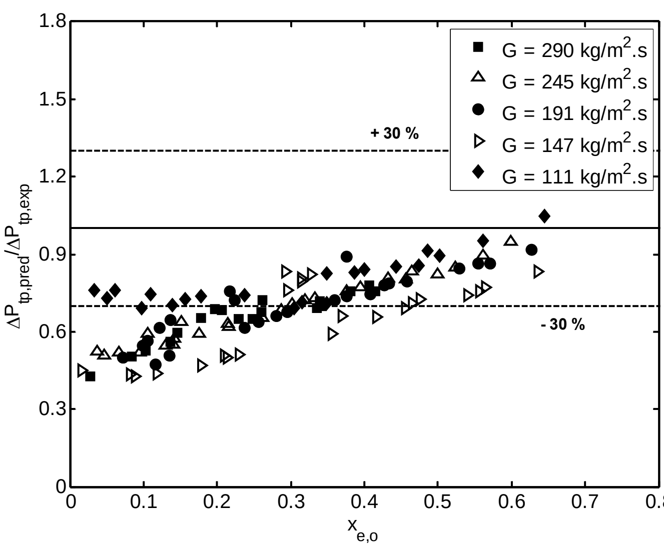

Figure 7. Comparison between the present measurements and the correlation by Lee and Garimella [14].

Figures 8 and 9 show amplitude oscillations of typical instability data of inlet pressure, outlet temperature, and mass flux acquired at a sampling rate of 2 for 500 seconds. The oscillating inlet pressure amplitude dissipates with increasing mass flux as shown in Fig. 8.a. The results also show that the amplitude value at low mass flux is about three times the amplitude value at higher values of mass flux. At the same time, the oscillation period of inlet pressure increases at low mass flux and presents a long oscillation period of about 14 seconds. This phenomenon is consistent with the results of Huh et al. [15] and Wang and Cheng [16], in which the amplitude of pressure drop oscillations rises significantly at a lower mass flux. The influence of the mass flux on the instability outlet saturation temperature is shown in Fig. 8.b. The amplitude and frequency of saturation temperature oscillations rise at low mass flux as shown in the figure. It is found that the oscillation amplitude decreases when the mass flux is higher, which means that the flow becomes more stable. The amplitude of this wave is about seven times higher than the amplitude of waves at a higher mass flux with an oscillation period of nearly 11 seconds.

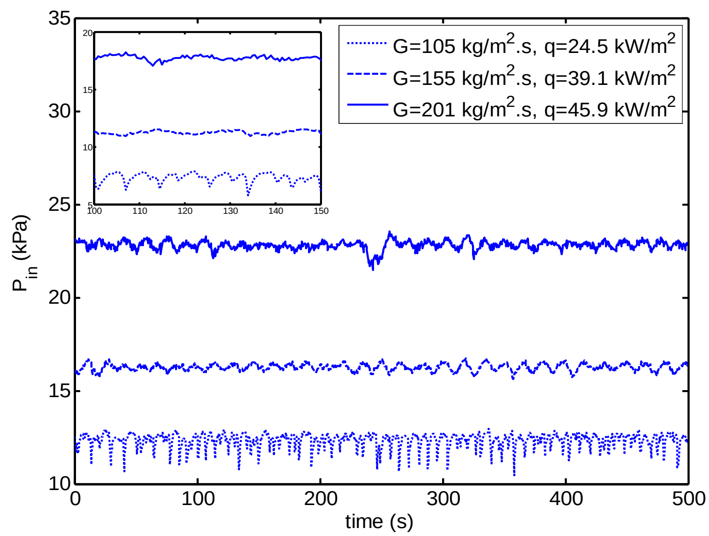

(a)

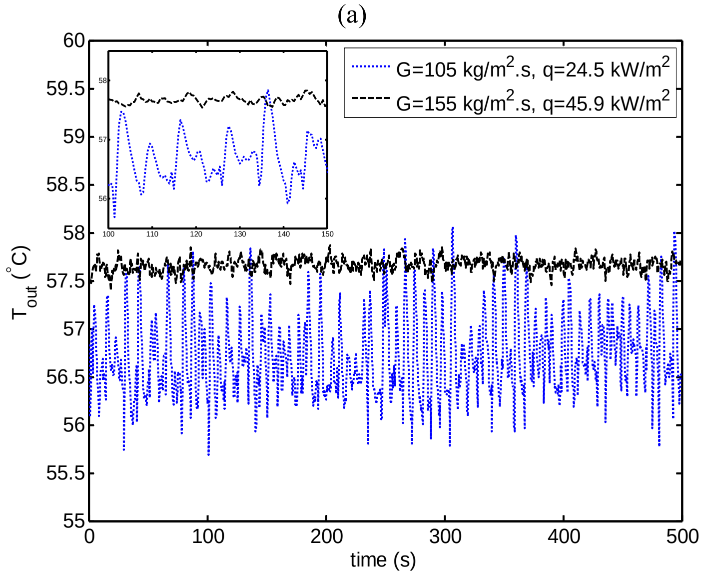

(b)

Figure 8. Oscillations of inlet pressure and outlet temperature measurements, q = 24.5 – 45.8 kW/m^2, and G = 105 - 201 kg/m^{2}s.

Mass flux instability at various heat fluxes is shown in Fig. 9. It was also found that most of the mass flux instability occurred at higher mass flux. As is evident from the figure, there is no clear trend representing dominant frequency and amplitude of the frequency. These inlet pressure amplitudes are almost half of those presented by Muwanga et al. [5] for flow boiling in cross-linked microchannel heat sinks using water, while the present oscillation periods are longer. On the other hand, the data recorded by Muwanga et al. [5] showed that the outlet temperature oscillates with higher amplitudes compared to the present study. Nonetheless, the outlet temperature periods of oscillation exhibited in Fig. 8.b are found to be longer than the oscillation periods previously presented by Muwanga et al. [5]. Pan and Chang [17] provided experimental data on flow boiling instability of de-ionized water microchannel heat sinks. Their results showed that significant pressure drop oscillations appear at unstable conditions. With the aid of flow visualization, they found that the large pressure drop oscillations could be attributed to the length of bubble slugs growing and shrinking within the channel.

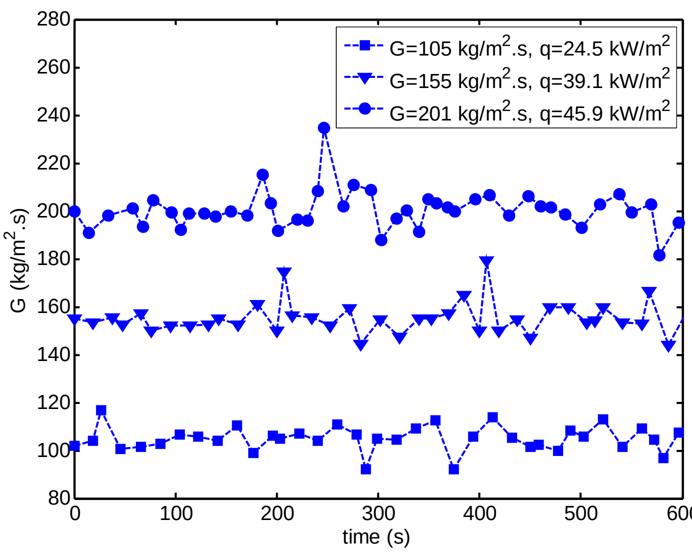

Figure 9. Mass flux oscillations, $q = 24.5 – 45.8$ kW/m^2, and $G = 105$ - 201 kg/m^{2}s.

CONCLUSIONS

Flow boiling characteristics of FC-72 were experimentally investigated in a cross-linked microchannel heat sink with a hydraulic diameter of 248 µm. Flow in the cross-links and the microchannels is visualized for the evaluation of cross-links effect on flow distribution as well as flow characteristics in the cross-links. Flow visualization experiments demonstrated that the observed flow regime is predominantly slug over the range of experimental parameters investigated in the present study. Results showed that the instability increased when the mass flux is decreased. The inlet pressure and outlet saturation temperature oscillate with higher amplitudes as the mass flux decreases. The two-phase pressure drop through microchannel heat sinks with the cross-links is much higher compared to the straight microchannel heat sinks due to the cross-link effect. The comparison of the experimental frictional two-phase pressure drop data versus the predicted results from Lee and Garimella's (2008) correlation shows a 30 % mean absolute error.

NOMENCLATURE

A	heat transfer area for the three side heating
C_p	specific heat, J/kg.°C
G	mass flux, kg/m^2.s
H	height, m
h_{fg}	latent heat of vaporization, J/kg
L	length, m
$\dot{m}$	mass flow rate, kg/s
N	number
ΔP	pressure drop, Pa
Q_{net}	net heat input, W
Q_{input}	input power to the fluid, W
Q_{loss}	heat loss, W
q	net heat flux, W/m^2
T_{in}	manifold inlet temperature, °C
T_{sat}	saturation temperature, °C
t	fin width
W	width, m
x_e	vapor quality

Subscripts

a	acceleration component
ch	channel
dyn	dynamics
expt	experimental
fr	frictional component
o	outlet
pred	predicted
sat	saturated
sec	section
sp	single-phase
tp	two-phase

REFERENCES

1. Tuckerman, D.B., and Pease, R.F.W., 1981, "High-performance heat sinking for VLSI," IEEE Electron Device Letters, EDL-2(5), pp. 126–29.
2. Dang, M., Hassan, I., Muwanga, R., 2007, "Adiabatic two phase flow distribution and visualization in scaled microchannel heat sinks", Experiments in Fluids, 43(6), pp. 873-85.
3. Dang, M., and Hassan, I., 2008, "Adiabatic two-phase flow in scaled microchannel heat sinks with cross links," Journal of Thermophysics and Heat Transfer, 22(4), pp. 587-97.
4. Xu, J.L., Zhang, W., Wang, Q.W., Su, Q.C., 2006, "Flow instability and transient flow patterns inside intercrossed silicon microchannel array in a micro-timescale," International Journal of Multiphase Flow, 32(5), pp 568-92.
5. Muwanga, R., Hassan, I., and MacDonald, R., 2007, "Characteristics of Flow Boiling Oscillations in Silicon Microchannel Heat Sinks", Journal of Heat Transfer, 129(10), pp. 1341-51.

6. Cubaud, T., and Ho, C.-M., 2004, “Transport of bubbles in square microchannels,” Physics of Fluids, 16(12), pp. 4575-85.
7. Dukler, A.E., Fabre, J.A., Mcquillen, J.B. and Vernon, R., 1988, “Gas-liquid flow at microgravity conditions - flow patterns and their transitions,” International Journal of Multiphase Flow, 14(4), pp. 389–400.
8. Yadigaroglu, G., 1981, “Two-phase flow instabilities and propagation phenomena. In: Delhaye, J.M., Giot, M. and Riethmuller, M.L., Editors, Thermohydraulics of Two-Phase systems for Industrial Design and Nuclear Engineering, Hemisphere, Washington DC, pp. 353–403.
9. Bergles, A.E., Lopina R.F., and Fiori, M.P., 1967, “Critical-Heat Flux and Flow Pattern Observations for Low Pressure Water Flowing in Tubes,” J. Heat Transfer, 89, pp. 69–74.
10. Lee, J.D., and Pan, C., 1999, “Dynamics of multiple parallel boiling channel systems with forced flows,” Nuclear Engineering and Design, 192(1), pp. 31-44.
11. Mishima, K., and Hibiki, T., 1996, “Some characteristics of air–water two-phase flow in small diameter vertical tubes,” Int. J. Multiphase Flow, 22, pp. 703–12.
12. Lee, H.J., and, Lee, S.Y., 2001, “Pressure drop correlations for two-phase flow within horizontal rectangular channels with small heights,” Int. J. Multiphase Flow, 27(5), pp. 783–96.
13. Lee, J., and Mudawar, I., 2005, “Two-phase flow in high-heat-flux micro-channel heat sink for refrigeration cooling applications: Part I-pressure drop characteristics,” Int. J. Heat and Mass Transfer, 48(5), pp. 928–40.
14. Lee, P.S., Garimella, S.V., 2008, “Saturated flow boiling heat transfer and pressure drop in silicon microchannel arrays,” International Journal of Heat and Mass Transfer, 51(3-4), pp. 789-806.
15. Huh, C., Jeongbae, K., and Kim, M. H., 2007, “Flow pattern transition instability during flow boiling in a single microchannel,” International Journal of Heat and Mass Transfer, 50(5-6), pp. 1049-60.
16. Wang, G., and Cheng, P., 2008, “An experimental study of flow boiling instability in a single microchannel,” International Communications in Heat and Mass Transfer, 35(10), pp. 1229-34.
17. Pan, C., and Chang, K.H., 2007, “Two-phase flow instability for boiling in a microchannel heat sink,” International Journal of Heat and Mass Transfer, 50(11-12), pp. 2078-88.